Part-Span Approximation of Tone Noise Propagation in an Aeroengine Intake. Part II: Non-Linear Propagation

Joseph S. P. Binns*, Long Wu† and Alexander G. Wilson‡
Institute of Sound and Vibration Research, University of Southampton, Highfield, Southampton, UK SO17 1BJ

Part I of this study, reported separately, introduced a part-span approximation for linear propagation of fan tone noise in aeroengine intake ducts. Analytical and computational methods were used to understand how artificially changing the hub-to-tip ratio of a duct impacts the representation of acoustic modes and their propagation. In many representative cases, the approximation was successfully applied and potential sources of error were highlighted. This understanding is extended in the present paper to include non-linear effects. While conventional CFD methods can predict the acoustic field with reasonable accuracy, the computational expense is too high for iterative application during the design process. The research community also requires more efficient methods to understand modern challenges such as the impact of increased flow distortion with future UHBR (Ultra-High Bypass Ratio) designs. The effect of the part-span approximation is first assessed for high-amplitude acoustic waves in uniform ducts with uniform flow. The part-span approximation is then implemented for an axisymmetric, but otherwise realistic, intake geometry with non-uniform inflow and a realistic buzz-saw noise source. The results of this simulation are compared with results from a conventional full-span calculation. The approximation provides a significant saving in computational expense and successfully captures much of the acoustic content of interest.

I. Introduction

Tonal fan-related noise is becoming an increasingly important contribution to a turbofan engine's noise emissions due to recent and future engine design trends [1]. The present study investigates the propagation of tone noise in aeroengine intake ducts. Part I of this study, reported separately [2], included a broader introduction to the topic and its focus was linear propagation. In the present paper, non-linear, shock-associated noise propagation is considered.

At high-power operating points, the supersonic tip speed of the fan blade results in the formation of a bow shock at the leading edge and a Prandtl-Meyer expansion fan across the rear blade surface [3]. This induces a high-amplitude cut-on acoustic pressure field which non-linearly propagates upstream through the intake duct before radiating to the far-field. In the duct, the shocks rotate with the fan (rotor-locked) and, according to weak shock theory, propagate at the undisturbed speed of sound relative to the oncoming flow [4]. A fan with identical fan blades generates the same pressure wave at every blade passage, giving rise to discrete tonal noise at the Blade Passing Frequency (BPF) and its harmonics only. Realistically, there are small blade-to-blade variations due to manufacturing tolerances and wear. Particularly significant for shock generation is the variation in stagger angle that changes the flow capacity and the shock-detachment distance for each blade passage, affecting both the shock strength and propagation angle [5]. The consequent pressure field varies between each blade passage and repeats every full rotation of the fan, resulting in tonal components at every multiple of the fan rotation speed, or Engine Order (EO). This noise source is often called Multiple Pure Tones (MPT), or as in this paper, buzz-saw noise and has been widely investigated [1, 3–7]. This fan noise contribution is generally dominant in the forward arc during high-power conditions such as take-off, initial climb and the cutback condition. For fans operating in an entirely subsonic regime, such as during approach, tonal contributions from the fan are due to the periodic interaction of the rotor wakes with the stator, commonly termed Rotor-Stator Interaction (RSI) tones. These contributions are generally smaller than the broadband contributions but can still be significant. Their lower amplitude means that they propagate linearly through the duct. Linear propagation has been covered in depth in the sister paper of this study [2].

*PhD Candidate, Institute of Sound and Vibration Research, University of Southampton, Highfield, Southampton, UK SO17 1BJ.
†Research Fellow, Institute of Sound and Vibration Research, University of Southampton, Highfield, Southampton, UK SO17 1BJ.
‡Professor of Computational Aeroacoustics, Institute of Sound and Vibration Research, University of Southampton, Highfield, Southampton, UK SO17 1BJ.

In the intake duct, the acoustic field can be described as a sum of discrete acoustic modes related to the source, the duct geometry and the mean flow. The acoustic energy is often concentrated at higher-span regions depending on the combination of modes present. Hence, the opportunity to reduce the computational domain of large numerical calculations has been identified by only considering high-span regions of the intake and neglecting the region near the duct axis (with little acoustic energy). The first part of this study [2] considered this methodology for low-amplitude acoustic waves linearly propagating through ducts. In many applied cases, the part-span approximation was successfully applied, giving rise to limited error. In the limits of the method, such as for low circumferential mode orders and very high hub-to-tip ratios of the part-span domain, a more significant error was introduced. The error was categorised in three ways: source truncation error, in-duct propagation error and far-field radiation.

Linear approximations are not valid when considering the propagation of buzz-saw noise. As a result, the present paper extends the previous findings to non-linear, shock-associated tone noise propagation. First, a review of studies that have investigated the impact of flow distortion on tonal noise is presented. The relevance is to highlight the necessity for high-fidelity numerical calculations and their inherent high computational cost which makes them impractical for iterative use in the design process. Two test cases are then presented to evaluate the suitability of the approximation for different acoustic waves and in different applications, focusing on buzz-saw propagation in aeroengine intake ducts.

A. Impact of Flow Distortion

Future Ultra High Bypass Ratio (UHBR) turbofan designs [1] will have ducts with non-dimensionally larger diameters to improve fuel efficiency by increasing the ByPass Ratio (BPR) and decreasing the Fan Pressure Ratio (FPR). To maintain reasonable weight and drag characteristics, this will generally result in non-dimensionally shorter intake regions upstream of the fan [8]. The aerodynamic and noise implications are potentially large. One impact is the reduced axial region in which acoustic liners can attenuate propagating noise. Another is the increase in flow distortion at the fan stage and in the duct.

Many sources can contribute towards flow non-uniformities such as installation effects and flight conditions. With traditional intake designs, the level of flow non-uniformity can be reduced at the fan by manipulating the flow through the design of the intake duct. A shorter intake region inherently reduces the effectiveness of this.

Early studies of fan tonal noise concentrated on noise mechanisms with undisturbed flow [3–7, 9–12]. The undisturbed noise source mechanisms for RSI and rotor-alone noise are generally well understood, as well as the propagation mechanism when uniform conditions are assumed [4, 9, 13, 14]. The presence of flow distortion has been increasingly included in more recent studies.

It can be difficult to produce realistic flow distortion profiles in experimental settings. Schwaller et al. [15] is an example of early experimental work which considered the impact of steady inflow distortion using in-situ model aeroengine tests with axisymmetric and drooped intakes. These experiments were extended by Schwaller et al. [16] and showed that for the distorted (drooped intake) case there was a modal scattering effect. Inflow distortion is often described as a combination of low-order azimuthal modes k [17, 18]. For a transonic fan, the distortion interacts with the rotor-locked pressure field to produce noise at modes $m = nB \pm k$ (where $k = 1, 2, ...$) resulting in a pressure field consisting of many azimuthal modes, each with variations in amplitude and phase [19]. Schwaller et al.'s [15, 16] experimental work identified this interaction through data that was acquired by a microphone array far upstream of the fan in the intake and at locations outside of the duct. Consequently, while the effect could be identified, the physical understanding was very limited.

For this reason, computational studies are appealing due to their more complete representation of the flow and acoustic fields. The studies completed have used a variety of numerical methods, with some using non-linear CFD [18, 20–22] or linear Computational AeroAcoustics (CAA) [23], and others opting for hybrid coupling methods [17, 24–27]. Generally, the propagation and source effects have been considered using a decoupled approach (where they are calculated separately) and those who have completed coupled simulations face difficulties separating the effects during analysis. It is also not uncommon that simplifications are made to reduce the computational cost, but, in turn, neglect important effects.

Doherty and Namgoong's [20] numerical study considered the impact of steady distortion using a drooped intake. A stationary intake zone was coupled to a rotating fan domain using a sliding mesh and no geometry downstream of the fan was included. A staggered fan was considered at transonic regime, simulating a realistic buzz-saw noise source. A substantial portion of the work was validating the method with experimental data from a model fan rig where good agreement was observed. This simulation was considered 'state-of-the-art' and was designed for noise predictions up to the third BPF, though only validation at the first BPF was presented. Regarding noise, the drooped intake case resulted

in circumferential variation of the flow inducing a non-uniform relative Mach number and inlet angle for each blade, varying the shock strength at each leading edge. This resulted in non-uniform variations in Fourier amplitude at the first BPF both axially and circumferentially. The rotor-locked mode was observed to be scattered into neighbouring modes at the source, but more obviously during propagation through the heterogeneous flow field.

Around the same time, Daroukh et al. [28] demonstrated a fully installed numerical solution for turbofan tonal noise. Both upstream and downstream 3D effects were considered using a drooped intake and heterogenous OGV row with struts and pylons. The operating point was a subsonic regime so RSI was the focus of the study. Hence, a uniformly staggered fan was used. An overall noise increase of up to 3 dB was identified due to the distortion effect in both upstream and downstream directions. This work was further developed [22] to consider a transonic operating point. It was identified that the typical Tyler-Sofrin (TS) mode description [29] was no longer sufficient for tonal noise when distortion is included. The modal pressure field was observed to have much greater complexity with mode scattering during propagation and modification of the source. The source effect was highlighted as a variation of shock position along the chord of the blade. The shock mechanism was further altered by a variation in unsteady loading across each blade due to the distortion. Another study by Daroukh et al. [27] focussed on the impact of upstream and downstream distortion on shock generation and subsequent propagation. A uniformly staggered fan meant that the shock pattern was uniform across the blade row for the undistorted case inducing the rotor-locked $m = nB$ modes only. The azimuthal mode distribution at the BPF was shown to considerably vary for the distorted case. Close to the fan, the rotor-locked mode was scattered into somewhat nearby neighbouring modes and had significant amplitude. After propagating through the distorted intake flow field, the modal scattering was more extreme at the BPF.

Winkler et al. [17] used a hybrid CFD/CAA method first introduced by Winkler et al. [26] to predict the impact of a 3D drooped nacelle geometry on inlet and aft noise. The static test bed conditions meant that flow distortion was introduced both by the inlet asymmetry and heterogenous OGV row with bifurcations. The intake distortion could be well characterised by low-order azimuthal modes, while the downstream distortion had more complex modal contributions, albeit at a relatively lower amplitude. Their analysis tracked the evolution of different modal components at the first BPF both upstream and downstream. The TS modes were dominant downstream but decayed quickly upstream of the fan. In the intake, the distortion interaction modes contributed significantly to the pressure field highlighting the impact of inflow distortion. This study highlighted the requirement for coupled and installed aeroengine noise simulations to accurately represent the acoustic field.

A linear CAA study by Prinn et al [23] investigated the impact of inflow distortion on far-field noise propagation. Different intake models were used which introduced different levels of distortion. It was found that even low levels of distortion significantly scattered the otherwise sole BPF tone into a wide spectrum of adjacent circumferential mode orders by the time it had propagated to the intake throat. The far-field propagation study also found that the distortion had a significant effect, particularly on the directivity of propagated noise. For the drooped intake, the noise was directed more skywards and to the sides. This study confirmed many of the similar findings from a semi-analytical study by Astley et al [30] who also included the effect of acoustically lined ducts.

B. Computational Expense

The motivation of this study is to address the high computational expense required to complete high-fidelity noise propagation CFD calculations. Table 1 highlights the computational expense of some of the studies reviewed in the previous section. For studies where multiple simulations were completed, only the most relevant case is considered. The method and capabilities of each study are also presented.

Simplifications, resulting in lower computational cost, are often made when considering isolated problems such as for an undistorted case at a subsonic operating point, or for a linear far-field propagation calculation as in Prinn et al's [23] study. However, for cases with three-dimensional and non-linear effects, studies have indicated the significance of incorporating a coupled domain in a fully non-linear CFD calculation, ensuring that combined effects are not overlooked [17]. The high expense of such calculations is highlighted by Darouk et al's [22] study which required around a million CPU hours worth of computation to achieve predictions up to the second BPF including upstream and downstream distortion. In industry, it is not realistic to complete a large number of iterative design simulations at this level of expense, and so decisions are currently informed by the limited data and understanding of the research community. Methods and strategies to reduce the computational expense are therefore sought after to advance the communities' understanding.

Author (Year)	Method (CFD/CAA/ Hybrid)	Mesh Size (m cells)	Cost (CPU hours)	Distortion (US/DS/B)*	Buzz-Saw (Y/N)	RSI (Y/N)	BPF
Doherty and Namgoong (2016) [20]	CFD	180	51,200	US	Y	N	1
Daroukh et al. (2016) [28]	CFD	70	NA	B	N	Y	1
Daroukh et al. (2019) [22]	CFD	570	1,000,000	B	N (RA)	Y	2
Winkler et al. (2014) [26]	Hybrid CFD/CAA	89.5†	NA	B	Y	Y	3
Prinn et al. (2016) [23]	CAA‡	8.5m DOF	50	US	Y	-	1

Table 1 Summary of some numerical studies for turbofan tonal noise analysis. For studies where multiple simulations were completed, statistics are presented for the most relevant case only. *US = Upstream, DS = Downstream, B = Both. RA refers to transonic rotor-alone noise for an identical blade row. † Mesh for CFD calculation. ‡ CAA calculation for intake propagation, where only half of the annulus was modelled and 900 GB of RAM was required.

C. Scope of the paper

The impact of a part-span approximation, as has been introduced in Part I [2], is further explored in the present paper to consider non-linear propagation effects. Non-linear CFD methods are applied for two test cases. High-amplitude single-frequency (together with harmonics) propagation is first considered in uniform ducts. Then, a realistic buzz-saw noise source from a turbofan blade row is propagated through an axisymmetric, but otherwise realistic, intake geometry operating at a non-zero angle of attack.

In many applied settings, the tonal acoustic content of most interest in an aeroengine intake duct is concentrated at high-span regions, as has been demonstrated in Part I. The work completed considering linear propagation highlighted the successful application of a part-span approximation for many low-amplitude single-frequency tonal acoustic waves. In reality, the tonal buzz-saw noise content from a fan in a turbofan duct is high-amplitude and propagates non-linearly. As a result, the present paper aims to apply the approximation for high-amplitude signals in simple cases as well as complex, realistic cases.

The previous work highlighted a series of potential errors that can be introduced by a part-span approximation. These were categorised in three ways; source truncation error, in-duct propagation error and far-field radiation error. The first two are considered in the current paper. The previous findings are used to inform expectations and potential reasons for discrepancies introduced by the methodology.

The final, more realistic case is compared against a calculation completed by Wu and Wilson [31] which applies a more conventional propagation CFD method for the same geometrical and flow conditions.

II. Test Cases

Following the analysis from the first paper (Part 1), non-linear effects are now considered using two test cases:

- **A** CFD for Non-linear Propagation in a Uniform Annular Duct with Uniform Mean Flow
- **B** CFD for Tone Noise Propagation in a Turbofan Axisymmetric Intake Operating at Non-Zero Angle of Attack

The final case demonstrates the application of the approximation for a more realistic case and is hence compared with data from a conventional full-span methodology CFD calculation.

A. CFD for Non-Linear Propagation in a Uniform Annular Duct with Uniform Mean Flow

The first test case implements a URANS CFD method to non-linearly propagate an analytically generated acoustic mode through a uniform annular duct with uniform mean flow. The impact of a part-span strategy is assessed by varying the hub radius (r_h) of the duct, thus changing the hub-to-tip ratio (ν).

1. Method

The commercial software Ansys Fluent was used with an implicit and inviscid solver. To reduce computational expense, an azimuthal segment of the duct was considered using periodic boundary conditions at both side walls. In turbomachinery CFD, this is often termed a 'single-blade passage' calculation and can be used for the analysis of noise from a uniformly staggered and identical blade row. Since the pressure field in each blade passage is periodic, only azimuthal mode orders which are multiples of the input mode order can be understood. A diagram of a domain for different azimuthal harmonic indexes m is presented in Figure 1.

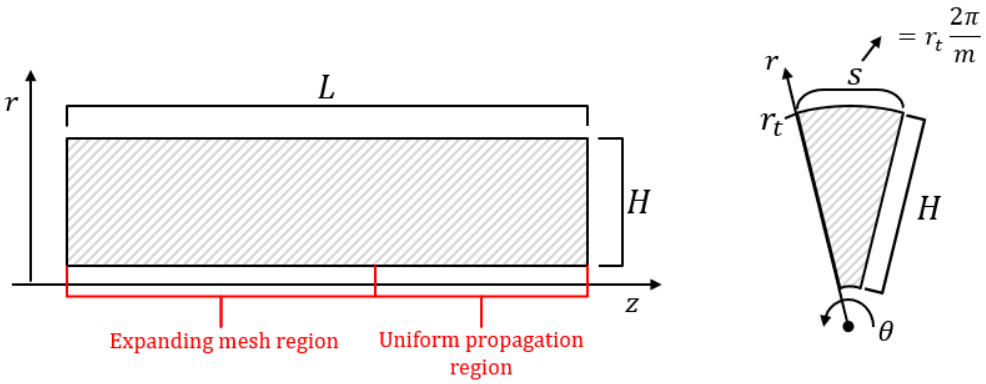

Fig. 1 Planar diagrams of the geometry used in the simplified CFD calculation.

Sim #	Azimuthal mode index (m)	Hub-to-tip ratio (ν)
1a)	6	0.2
1b)		0.5
1c)		0.75
2a)	11	0.2
2b)		0.5
2c)		0.75
3a)	22	0.2
3b)		0.5
3c)		0.75

Table 2 Simulation matrix for test case A.

Three different circumferential mode numbers are considered, all for the first radial harmonic, and three hub-to-tip ratios, as highlighted in the simulation matrix in Table 2. A 'rotor-locked' pressure field is simulated such that the rotational frequency of the signal ω is a function of the circumferential mode number m and a theoretical 'shaft rotation frequency' Ω, such that $\omega = m\Omega$. The input signal was generated according to the method derived in Part I of this study [2], such that the pressure p is given by,

$$p(r, \theta, z, t) = p_{m,n}(r) e^{-im\theta} e^{-ik_z z} e^{i\omega t}, \tag{1}$$

where r is the radius, t is time, m is the circumferential harmonic index, n is the radial harmonic index and k_z is the axial wavenumber. The shaft frequency Ω was selected such that the pressure field's relative motion toward the duct's outer radius was supersonic, ensuring a cut-on pressure field. For these cases, the freestream Mach number was 0.61. These values were chosen to simulate typical high-power operating conditions of a turbofan engine. The amplitude of the acoustic input signal was 170 dB (re 2×10^{-5} Pa) which is comparable to the amplitude experienced just upstream of a fan operating in the same condition. The cases with the high circumferential harmonic number of ($m =$) 22 may be likened to the rotating pressure field from a fan with 22 identical blades with a supersonic tip speed.

The largest domains had a hub-to-tip ratio of (ν =) 0.2, which is typical of the source position immediately upstream of the fan's leading edge in a turbofan engine. For the most part, this is referred to as the full domain datum case throughout the discussion. Two part-span domains are considered at hub-to-tip ratios of 0.5 and 0.75, where the tip radius of the duct remains constant across all domains.

As was suggested in Figure 1, the computational domain is split into two sections axially; a propagation region, and an expanding mesh zone. In the propagation region, uniform spacing of axial and circumferential cells with a resolution of at least 20 PPW at 3BPF has been considered sufficient to ensure the decay due to numerical dissipation (for the frequencies of interest) is negligible when compared to non-linear decay [32]. This has been validated in multiple comparable studies [33, 34]. Even for non-linear propagation of the first BPF, a mesh density up to three times as dense as one required for linear propagation is needed due to the redistribution of acoustic energy into different harmonics of itself [3, 4]. For example, in the case of an $m = 22$, $n = 1$ high amplitude pressure wave, energy will redistribute into the $m = 44,\ 66, \ldots$ modes as well as different radial harmonic orders. The axial length of the propagation region was scaled such that for the first radial harmonic, seven axial wavelengths were capable of being resolved.

Regular, structured computational meshes were designed using ICEM CFD. A resolution sufficient to accurately resolve the acoustic content was achieved according to the input signal's frequency. In the axial direction (z), 120 points per theoretical wavelength (PPW) were used and 140 PPW in the azimuthal (θ) direction in the propagation region. Table 3 highlights the mesh size for each domain.

Hub-to-tip ratio ν	**Mesh size (nodes)**
0.2	11×10^6
0.5	6.5×10^6
0.75	3×10^6

Table 3 Mesh size information for the non-linear uniform duct CFD calculations.

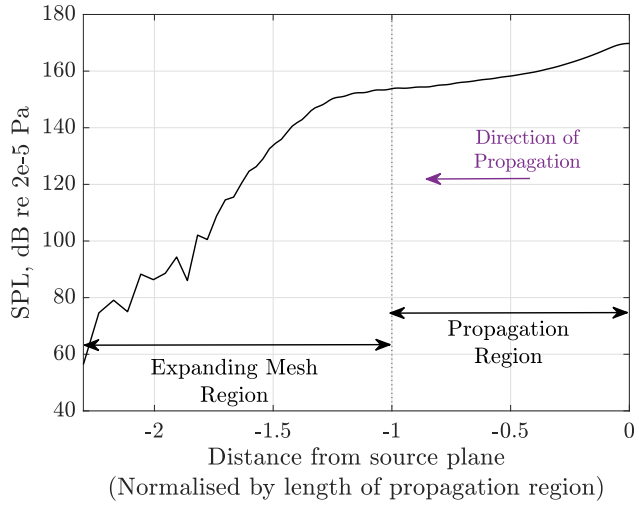

Fig. 2 A plot of Sound Pressure Level (SPL) in dB (re 2×10^{-5} Pa) plotted against axial distance showing the amplitude of the first radial harmonic from the $m = 22$, $\nu = 0.2$ case highlighting how an expanding mesh region sufficiently decays the signal as it propagates after the uniform region.

To minimise unwanted reflections of acoustic waves from the inlet boundary, a region of expanding mesh was designed upstream of the propagation region. The expansion rate was 1.05, and once again, the axial length was designed so that the most upstream cell had a resolution of 2 PPW (axially). This region gradually dissipates the upstream travelling acoustic wave so that it has no (or very little) amplitude at the inlet boundary. This is shown in Figure 2 for the full domain $m = 22$ case, where the amplitude quickly decays upstream of the propagation region. Throughout the discussion, only the uniform propagation region is considered.

In the radial direction, a uniform mesh spacing was used as an inviscid turbulence model was used. Hence, a boundary layer mesh at the walls was not required.

The solution was iterated towards a steady state using an instantaneous snapshot of the acoustic pressure field at the outlet boundary and a second-order upwind spatial discretization scheme. For the transient solution, a second-order implicit time discretization scheme was used where each time step had 10 inner iterations achieving inner convergence of at least 5 orders. The pressure outlet boundary condition was updated after each time step according to the analytically computed pressure field. A time step around 3×10^{-6}s with 8000 time steps for each full rotation (of the full annulus) was deemed sufficient to represent the shock discontinuity accurately. The number of time steps required to propagate the acoustic wave through the domain sufficiently was frequency-dependent and varied for each case. For the highest circumferential mode number of (m =) 22, two full rotations of the boundary profile were required, whereas, for the lowest circumferential mode of (m =) 6, at least five rotations of the profile were needed as a result of the lower group velocity at this harmonic and frequency.

2. Expected Findings according to Linear Theory

Part I of this study, where linear propagation was concerned, identified seven potential sources of error due to the part-span approximation. They were categorised in three ways: source truncation errors, in-duct propagation errors and far-field radiation errors.

Source truncation errors relate to the representation of the initial pressure profile in terms of acoustic modes in the part-span region. It was found that the error introduced here was most significant when a significant amount of the signal power was truncated and for cases close to the cut-off/cut-on boundary. For the linear cases, the source truncation error occurred over a small initial propagation period and remained constant during the wider propagation.

In-duct propagation errors grow over the propagation distance and are related to the axial wavenumber variation introduced by the part-span approximation. A phase error was introduced for cases with a single cut-on mode, while if there were multiple cut-on modes, the biggest error was likely in directivity. Given this test case only considers the in-duct region, the third type of error, far-field radiation errors, is not considered.

In non-linear cases, any amplitude error introduced by the part-span approximation is expected to have a diminished effect over propagation. As suggested by 2D non-linear decay theory [3, 7], signal decay is relatively insensitive to initial amplitude, provided it is in the non-linear region. Therefore, any disparity in amplitude introduced at the source plane (due to profile truncation and the introduction of amplitude in high-order radial modes, which are cut-off) is expected to have little effect on the propagated amplitude.

Regarding phase error, even if different modal components of a propagating signal exhibit different phase variations, the most significant is anticipated to be that of the first harmonic. Consequently, it may be possible to understand the overall phase error by only considering the first harmonic, though this is evaluated later.

Far-field radiation errors are not considered in this study but relate to the impact of a part-span inner wall in the far-field domain.

3. Results

Before the findings from each case are presented, and the impact of a part-span approximation is considered, a Fourier-Bessel wavesplit method, as presented by Wilson [35], is applied to the simulation data. This allows for the acoustic field to be decomposed into its components and isolate the upstream and downstream travelling acoustic waves. Only an upstream travelling acoustic wave is used as the input for these simulations, but the presence of boundaries and an upstream expanding mesh may introduce reflections.

For case no. 3a ($m = 22$, $\nu = 0.2$), the upstream and downstream amplitudes of the first and second radial components of the $m = 22$ mode are shown in Figure 3(a). Initial observation highlights that the amplitude of the downstream component is small (< 30 dB) compared to the upstream one, as expected. The significantly low amplitude means that these downstream amplitudes are not reliable and should be considered negligible. The components are likely due to leakage from other modal components as a result of the limitation of the method which assumes the relationship between pressure and velocity will be exactly the same as that computed in the CFD code [35].

The amplitude of the second upstream radial harmonic of the input mode ($m = 22$) is shown to initially gain amplitude as energy from the first radial harmonic redistributes into the second. The second upstream radial harmonic is cut-on (albeit close to the cut-off boundary), and hence should propagate at constant amplitude according to Tyler and Sofrin's linear method. Figure 3(a) highlights that its amplitude varies over the propagation region.

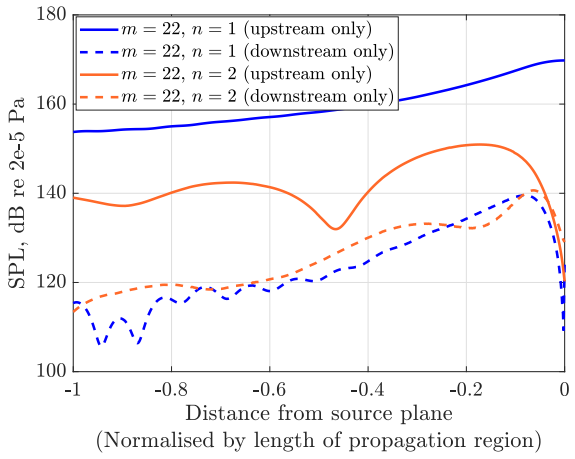

(a) The upstream and downstream amplitudes (SPL) of the first and second radial components of the m = 22 circumferential mode.

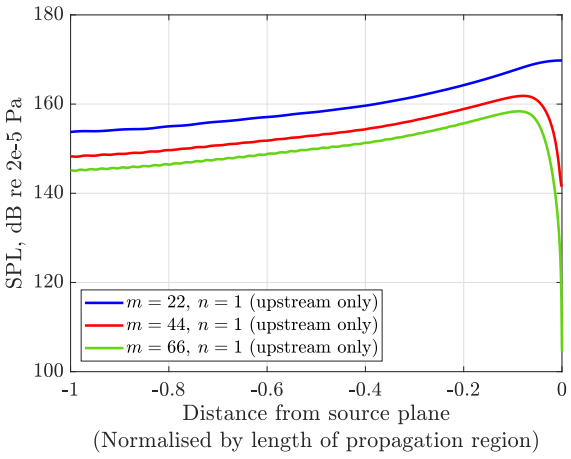

(b) The upstream amplitudes of the m = 22, m = 44 and m = 66 circumferential mode harmonics, all for the first radial harmonic.

Fig. 3 Amplitudes following a Fourier-Bessel wavesplit for case no. 3c, where the input circumferential mode number is (m =) 22 and the hub-to-tip ratio is (ν =) 0.2, the baseline duct size.

Given the high amplitude of the input signal at m = 22, during initial propagation, a shockwave forms. As well as distributing energy into other radial harmonics, acoustic energy is also redistributed into circumferential harmonics of the original mode. This is highlighted in Figure 3(b), where the amplitudes of the upstream components at the original circumferential mode and two of its harmonics (for the first radial mode) are shown. The input mode m = 22 starts at around 170 dB and decays non-linearly upstream. For the harmonics, the amplitude rises initially as the energy redistribution occurs and then they decay similarly to the original mode, albeit at a lower amplitude.

Similar observations were made for all three circumferential mode number inputs with the datum hub-to-tip ratio case. The aim of this section, however, is to understand the impact of the part-span approximation on non-linear propagation. So the focus now shifts to comparing the findings of different duct hub-to-tip ratios.

The shock profile along the duct outer wall is considered first. After propagating halfway through the propagation region axially (around 3-4 axial wavelengths), the static pressure on the outer wall of each duct is plotted against azimuthal position in Figure 4(a) for the cases with a circumferential harmonic index of (m =) 22. A similar shock pattern is shown for all three hub-to-tip ratios, though there are observable differences. The most obvious is a 'bulk' phase variation between each case. While noticeable in plots like this, in many acoustic calculations, amplitude prediction is the objective and this bulk error can often be ignored.

Also noticeable in this plot is a slight difference in amplitude between the cases. However, this effect is minor, especially once converted to a perceivable metric such as decibels. The findings of the linear section of this study suggest that at a high circumferential harmonic like this, the effect of the part-span approximation should be small.

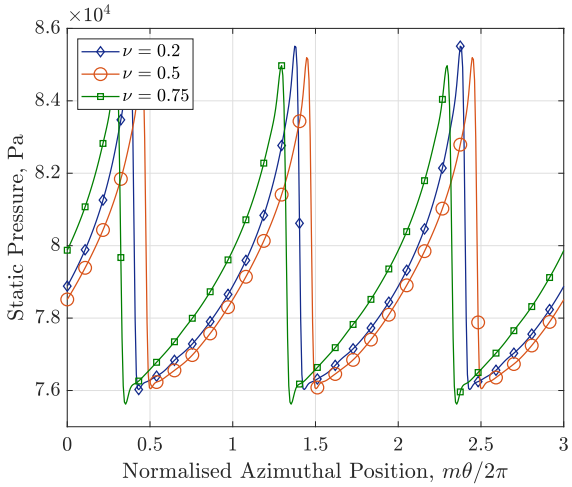

(a) Static pressure plotted against normalised azimuthal position on the duct outer wall 3.5 axial wavelengths upstream of the source position.

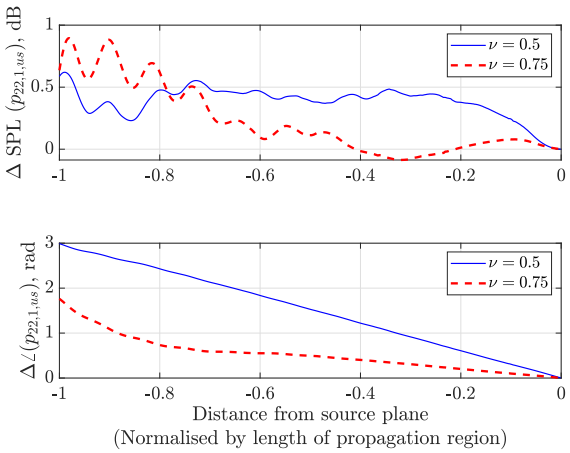

(b) Amplitude (top) and phase (bottom) difference between the datum and part-span ducts for the first upstream radial harmonic of the input circumferential mode (m = 22) as the signal propagates through the propagation region.

Fig. 4 Data presented for the circumferential order of (m =) 22 in all three duct geometries of the first test case.

To further investigate the error introduced by the part-span approximation for this circumferential harmonic, the difference in amplitude and phase of the first upstream radial harmonic of the input mode is shown in Figure 4(b) for both part-span domains compared against the datum duct. The first observation highlights how the variation in amplitude between the ducts is very small, reaching a maximum of 1 dB after propagating a distance of 7 axial wavelengths. In terms of phase variation, for the duct with a hub-to-tip ratio of (ν =) 0.5, there is a phase difference that increases at a constant rate during propagation. After propagating through the region, this component has a phase shift close to π radians. For the higher hub-to-tip ratio duct with ν = 0.75, the phase difference varies at a slower, but non-constant rate. This indicates that the error may vary during propagation even at this high circumferential harmonic, with a high hub-to-tip ratio.

For the other circumferential harmonics considered, the shock profile is shown mid-way through the propagation region in Figure 5.

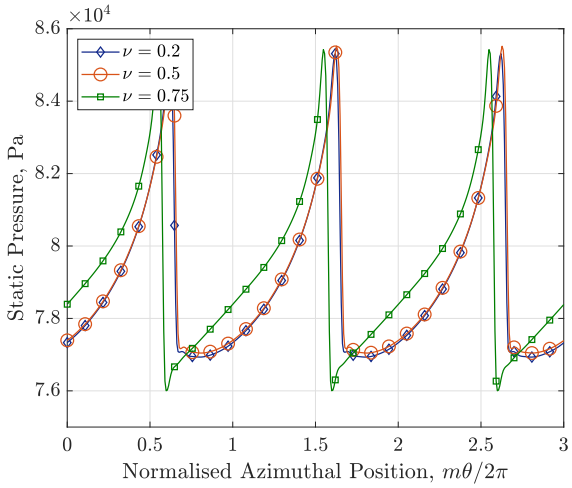

(a) m = 11

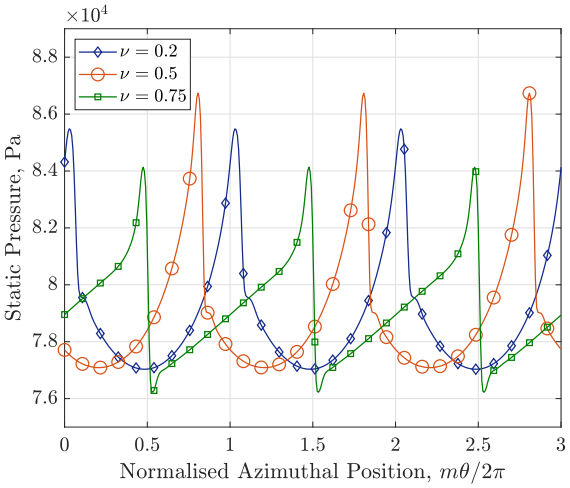

(b) m = 6

Fig. 5 Static pressure plotted against normalised azimuthal position on the duct outer wall 3.5 axial wavelengths upstream of the source position, shown for simulations with azimuthal input index of m = 11 and m = 6.

For the $m = 11$ case, the part-span domain has little-to-negligible impact on the propagated shock wave profile, suggesting the approximation at these hub-to-tip ratios may be suitable. For the extreme hub-to-tip ratio ($\nu = 0.75$), the biggest notable difference is a phase shift. The shock wave is also observed to appear more as would be expected from a 2D shock profile for this domain.

The linear work presented in Part I of this study [2] highlighted that the impact of a part-span approximation would be more significant on lower circumferential harmonics. Figure 5(b) shows the shock profile along the casing wall for the $m = 6$ circumferential harmonic case, the lowest m number in this series of simulations. The shock pattern notably varies for each hub-to-tip ratio.

It is noted at this point that the $m = 6$ case is not indicative of a signal that would be solely present in a typical turbofan application. While with a realistic buzz-saw noise source, there are components at circumferential harmonics as low as this, they are not as high amplitude and do not propagate independently in the intake duct.

The $m = 6$ case does, however, indicate the impact of a part-span approximation on high amplitude tonal inputs at lower circumferential orders. It is difficult to make sense of the effect purely by observing the shock profiles on the duct wall. A Fourier-Bessel wavesplit allows for further investigation. Figure 6(a) presents the amplitude and phase difference of the first upstream radial harmonic of the fundamental circumferential mode ($m = 6$) compared for both part-span domains with the datum duct.

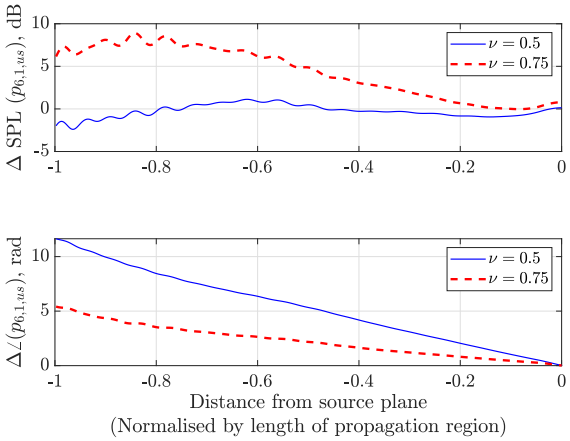

(a) Amplitude (top) and phase (bottom) difference between the datum and part-span ducts for the first upstream radial harmonic of the input circumferential mode ($m = 6$) as the signal propagates through the propagation region.

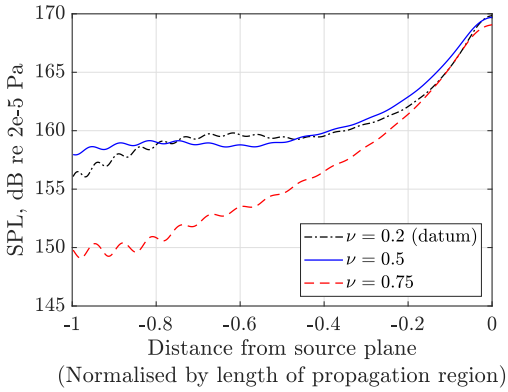

(b) The amplitude plotted along the propagation region for the first harmonic of the input circumferential mode for the three duct geometries.

Fig. 6 Data presented for the lowest circumferential input mode ($m = 6$) considered in this test case.

Considering the variation in amplitude for the part-span domain with hub-to-tip ratio of 0.5, the delta with the datum duct is relatively small, with a maximum of 2 dB at the end of the propagation region. While this is larger than has been observed for the other circumferential modes, over a propagation length of seven axial wavelengths, this may still be an acceptable amplitude error. For the higher hub-to-tip ratio of 0.75, the delta is more significant, with a maximum delta of around 8.5 dB. This is further noticed in Figure 6(b) where the amplitude of the first upstream radial harmonic of the $m = 6$ mode is plotted along the propagation region. The $\nu = 0.75$ case is shown to decay more significantly during propagation. There is also a noticeable difference in initial amplitude at the source plane ($z = 0$) due to truncation of some of the signal's power.

The phase variation introduced by the part-span domain is also more significant at this circumferential harmonic, as presented in Figure 6(a). This is due to the part-span approximation affecting the value of the real component of the axial wavenumber. In the datum duct, the axial wavenumber is computed as -7.60, while in the part-span ducts, the values were -7.65 and -8.48 for the hub-to-tip ratios of 0.5 and 0.75 respectively. This effect has been previously highlighted in the linear part of the study. While the greatest variation in the value is for the $\nu = 0.75$ case, Figure 6(a) highlights that the phase variation is actually greatest for the $\nu = 0.5$ case. The reason for this is unclear from the current analysis, though the significant error in amplitude would likely make this high hub-to-tip ratio case impractical if the calculation objective were for predictions at this circumferential harmonic.

B. CFD for Tone Noise Propagation in a Turbofan Axisymmetric Intake Operating at Non-Zero Angle of Attack

The second test case presented in this paper is a non-linear CFD calculation, implementing the part-span approximation, for the propagation of a realistic buzz-saw noise source through an axisymmetric aeroengine intake operating at non-zero angle of attack.

1. Method

Given the scale of this calculation, only a single part-span domain was considered, with a hub-to-tip ratio of (ν =) 0.5, defined at the source plane. The 'inner wall' of the part-span domain was specified by a streamtube from a steady 'coarse mesh' calculation. The 'coarse mesh' calculation had a resolution only sufficient to capture the flow and not the acoustic field in the intake domain, hence making it relatively cheap to run steady-state. In the fan domain, the mesh was sufficient to resolve the fan source, and details of the mesh are presented in Wu's paper [31]. A circular distribution of streamline seeds, with the same resolution as the mesh azimuthally, were positioned at the source plane (axially) and propagated upstream to the domain extent. These streamlines were then used to form a streamtube which defined the part-span domain inner wall. The flow condition was non-axisymmetric and a small angle of attack inflow of 3.57-degrees was imposed. Hence the streamtube was also non-axisymmetric.

This calculation concerned only the propagation through the intake region. The source was attained from a different calculation presented in Wu and Wilson's study [31]. The intake geometry is axisymmetric and consistent between the calculations. In Wu's calculation, a staggered fan with an axisymmetric OGV (Outlet Guide Vane) achieved a realistic buzz-saw noise source. The mesh was sufficient to resolve the source and propagate it through the in-duct region at frequencies up to the third blade passing frequency (BPF). Wu's study simulated a case with distorted inflow at the same angle of attack as the one concerned here. This simulation is used as validation for the present work. Wu and Wilson [31] also considered an undistorted flow field with zero angle of attack which was a datum case. Their work found that at the source plane, which was defined as the interface between the rotating and stationary domains, the impact of this low degree of flow distortion was minor on the source. Consequently, the source used in the present work is the one from the undistorted datum case. As mentioned in the further works section, the intent is to extend this part-span methodology to a coupled approach.

For the present calculation, the computational domain extends to the far-field in the radial and axial directions by at least 10 fan diameters. The computational mesh was designed in ICEM CFD and had a resolution in the intake very similar to that in the validation calculation of Wu and Wilson [31]. Azimuthally, there were around 1800 nodes, 270 nodes axially (from the source plane to the highlight), and around 80 points radially in the duct. The mesh had around 80 million cells, around 70% of the cell count for a mesh used in the intake region for a full domain calculation which represents the same acoustic resolution. The in-duct region of the mesh is shown in Figure 7.

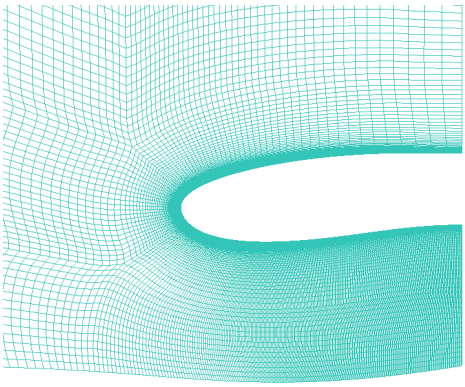

Fig. 7 An azimuthal plane of the intake mesh used for the part-span approximation calculation.

Ansys Fluent was the chosen solver for the propagation calculation, as for test case A. The flow conditions were specified at the external boundaries using free-stream characteristic boundary conditions, specifying the static pressure, Mach number and flow direction, and total temperature. The 'inner wall' of the part-span domain was defined using a streamtube as earlier explained, and the boundary condition was a slip wall condition, hence having zero impact on the flow field. A no-slip wall boundary condition was used for the outer wall of the intake duct. The internal downstream

boundary in the duct specified the source, attained from the calculation of Wu and Wilson [31]. An unsteady boundary condition was implemented where the static pressure profile was specified at every time-step, as in the first test case of this paper. The flow field was iterated towards a steady state using an instantaneous snapshot of the pressure field at the outlet boundary and a second-order upwind spatial discretization scheme. For the transient solution, a second-order implicit time discretization scheme was used. A full rotation of the source consisted of 1600 time steps, and 10 iterations were required at each time step to achieve convergence of flow variables. The CFD solver applied in the validation calculation of Wu and Wilson [31] was different to Ansys Fluent, though both codes are low-order finite volume URANS solvers and both apply the same turbulence model for this case (Spallart-Allmaras). Six full rotations of the source were completed for the part-span calculation.

For post-processing, comparison with the full-span calculation, and analysis, the CFD solutions were interpolated onto a regular r-theta grid which was identical for both cases. As a result, data is only presented in the part-span calculation for both cases, even though the validation calculation (often called baseline calculation throughout the discussion) implemented a more typical full-span methodology, as presented by Wu and Wilson [31].

2. Flow Validation

Before the acoustic results are considered, the simulated mean flow is presented. Given the part-span approximation, it is important to ensure that the methodology has little impact on the mean flow, which could lead to significant effects on acoustic propagation. This is understood by comparing the flow field of the present calculation with the mean flow of the equivalent simulation in Wu and Wilson's [31] study with the same intake geometry and angle of attack. The mean flow of the validation calculation is the time-averaged mean flow from the unsteady calculation. This is compared against the converged steady-state calculation applying the part-span methodology. Limited differences are anticipated as a result of small variations in the approaches. Likely the most significant is that, in Wu's simulation, a fully coupled approach, with a distorted fan source is applied, whereas the present part-span calculation uses an undistorted source. While this effect was determined to be minor in Wu's findings, it may still have a small effect on the mean flow, and hence the acoustic results.

First presented in Figure 8 is a static pressure contour plot along the surface of the nacelle, where $\pi/2$ radians refer to the top of the nacelle and $3\pi/2$ radians refer to the lower lip of the nacelle. The effect of the flow distortion is clear, highlighting a greater acceleration of the flow at the bottom lip. The dashed contour shows the mean flow from the part-span approximation calculation, and very minor, almost negligible, differences are presented. The differences are slightly greater towards the source plane, as would be anticipated given the slight variation in source profiles.

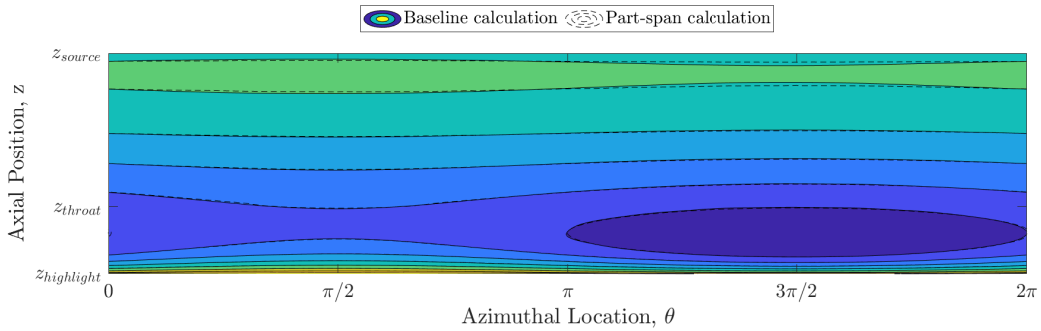

Fig. 8 Contour plot of the mean flow static pressure on the intake duct outer wall for the baseline (–) and part-span (- -) calculation.

The difference on the source plane can be appreciated by considering the circumferentially averaged radial pressure profile (shown only in the part-span region) at the source plane, as is presented in Figure 9. Once again, it is shown that, in the part-span region, the discrepancies between the calculations are minor. It is noted, however, that circumferentially averaging the pressure in the validation case neglects the azimuthal effect of distortion introduced by the non-uniform inflow.

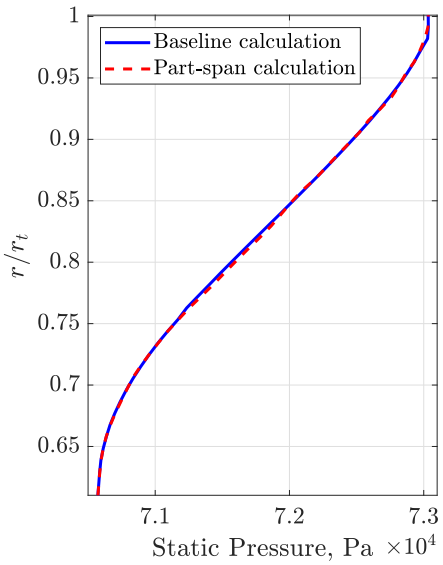

Fig. 9 Static pressure (in Pascals) plotted against radius (non-dimensionalised by the tip radius) showing the circumferentially averaged radial pressure profile at the source plane for the baseline (validation) calculation and the part-span calculation.

Consequently, the flow field can also be considered at different axial positions, as is presented in Figure 10. Axial cuts show the r-theta plane at the highlight, throat and source plane axial positions. At both the highlight and throat positions, the variation between the two calculations is very small, and the effect of the inflow distortion is well-captured by the part-span approximation. At the source plane, where small differences are anticipated, there are some minor variations between the calculations. While this may have an effect on the resultant acoustic propagation, it is expected that this will be small according to Wu and Wilson's study [31].

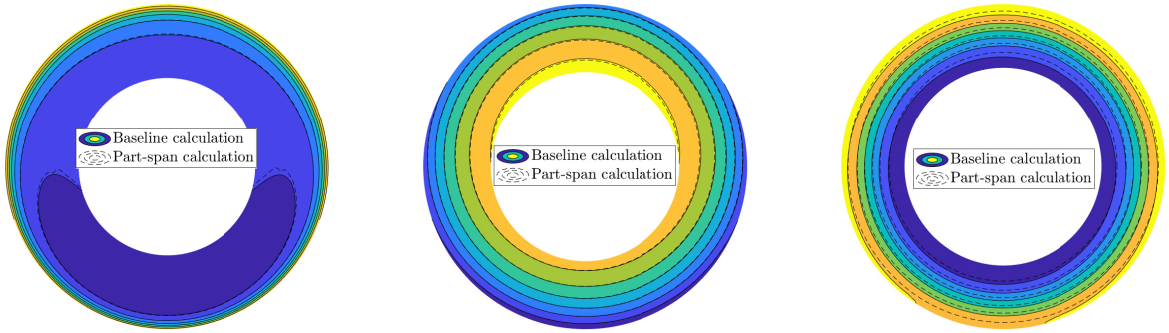

(a) Highlight axial position. (b) Throat axial position. (c) Source plane axial position.

Fig. 10 Static pressure contour plots of the mean flow at three axial positions for the baseline (validation) and part-span calculation. The time-averaged mean flow is presented for the baseline, and the converged steady flow is shown for the part-span calculation.

It has been determined that the distorted flow field can be accurately captured when applying the part-span approximation. It is noted, however, that when using an undistorted source, as is the current application, there are small variations towards the source plane which may introduce small errors in the acoustic propagation predictions. This is a possible limitation of the current calculation but could be addressed in the future by using a distorted source profile.

C. Acoustic data

The predicted acoustic field is now considered. Data are presented for both the part-span calculation and the full-span calculation. While a case with inflow distortion is presented, this section will not focus on its effect but rather on how the part-span approximation can resolve the distorted acoustic field, using the full-span calculation as a baseline. Wu and Wilson's study [31] presents a more in-depth analysis of the impact of inflow distortion for this case.

The first figure (Figure 11) shows instantaneous static pressure contour plots at two axial locations, the source plane and the intake throat. The stagger variation between each blade is notable at both locations and for both calculations as the shock strength varies at each blade passage. As expected, the source position (Figures 11(a)-11(b)) shows no notable difference between the calculations.

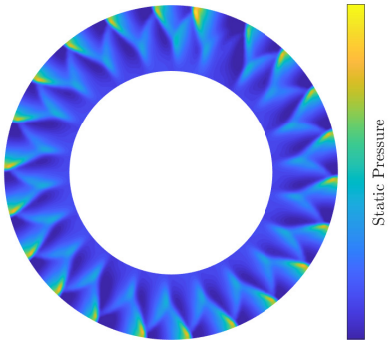

(a) Part-span calculation, source plane axial position.

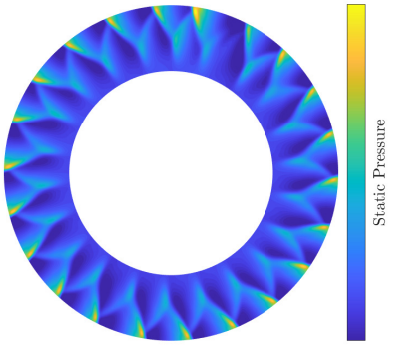

(b) Full-span calculation, source plane axial position.

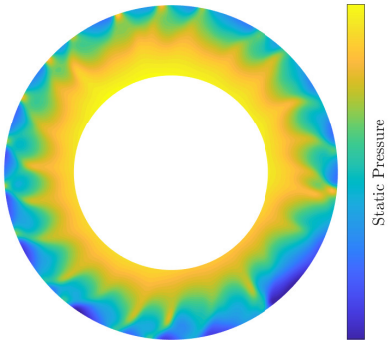

(c) Part-span calculation, intake throat axial position.

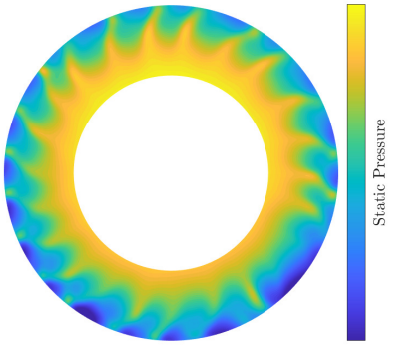

(d) Full-span calculation, intake throat axial position.

Fig. 11 Instantaneous contour plots of static pressure immediately upstream of the source plane (11(a)-11(b)) and the intake throat (11(c)-11(d)) for the part-span calculation and the full-span calculation.

Further upstream (Figures 11(c)-11(d)), the contours are also observed to be similar. The distorted mean flow field is highlighted by the greater region of low pressure at the bottom lip of the intake and is similarly represented in both cases. The propagated shock field is also observed to be similar in both cases. The main difference identified is the amplitude at higher radii appears higher (at some azimuthal positions) in the part-span calculation, though it is difficult to interpret solely using this contour.

The next instantaneous contour plots in Figure 8 show the static pressure on the intake duct outer wall for both calculations. The propagation of the shock field along the duct wall is shown in both cases, and the effect of the blade stagger angle is highlighted by its non-uniformity across the azimuthal position. Also highlighted in these contours is the flow distortion pattern and how it impacts the shock propagation, particularly at the lower lip of the nacelle ($3\pi/2$ radians). A potentially considerable difference between the two solutions is that, for the part-span calculation, the peak

amplitude of the shock field seems to maintain a higher level as it propagates upstream. In comparison, in the full-span calculation, the initial amplitude decays quickly and becomes somewhat less defined further upstream.

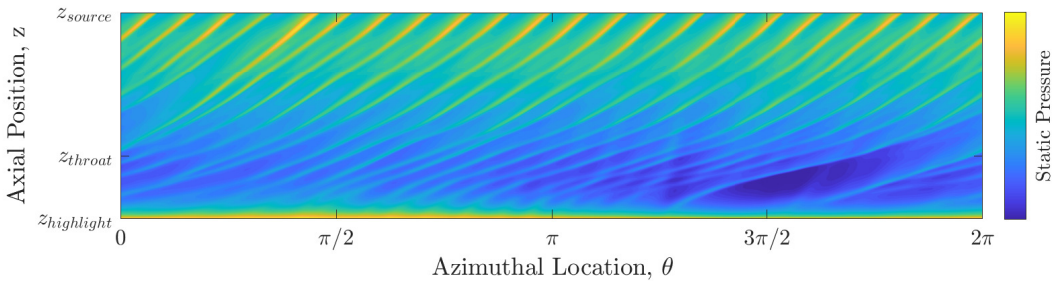

(a) Part-span calculation.

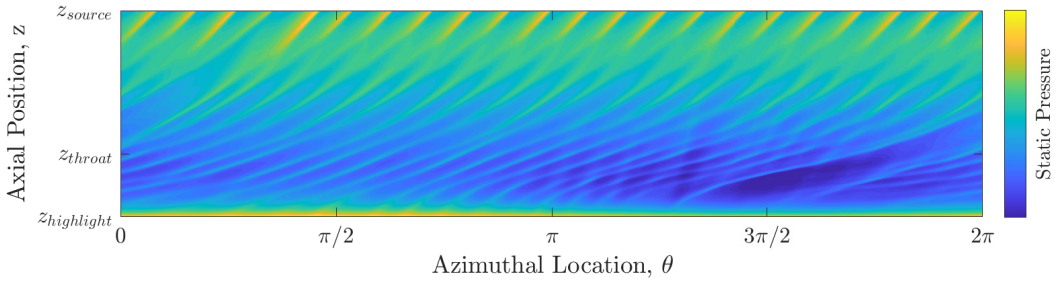

(b) Full-span calculation.

Fig. 12 Instantaneous static pressure contour plots (at different instances) showing the propagation of the shock field on the intake duct outer wall from the source position up to the highlight for both part- and full-span calculations.

While not a 'rotor-locked' field due to the inflow distortion, a spatial Fourier transform can be completed in the azimuthal direction at different axial positions, as presented in Figure 13 for both cases at 95% span.

Figure 13(a) shows a spectrum positioned upstream of the source plane by 5% of the duct radius. The amplitudes of the BPF tones are very similar between the cases. While there are small differences, the general shape of the buzz-saw tone amplitudes are also consistent. As the enquiry position is moved further upstream (to 50% of the duct outer wall radius, Figure 13(b)), the impact of the part-span domain becomes more apparent. The amplitude of the first BPF tone, at $m = 22$, is within 1 dB between the calculations. At the harmonic orders lower than $m = 22$, the predictions are generally within 3 dB down to $m = 5$. Below this, there are greater deviations (up to around 7 dB for $m = 3$). This is consistent with the linear work which has been completed and reported in Part I, and the simplified non-linear test case A of this paper (Section II.A), which showed that the part-span approximation has a greater impact on low circumferential harmonics because a larger proportion of the acoustic energy flux is excluded.

At higher circumferential harmonics ($m > 28$), significant deviations are observed. The reasons for this are not fully known. This result may be due to the part-span approximation itself, though this is not expected given the results previously presented in Part I [2] and test case A of this paper. Alternatively, this result may indicate that the part-span calculation is not fully converged and requires further iterations to sufficiently propagate the acoustic field through the duct. This is considered further in the discussion of Figure 15(b). Finally, it is worth noting that the CFD solvers used for the two calculations are different. Although both are finite volume codes, the handling of shock waves will be different. Any difference in shock-smoothing algorithm would be expected to have a disproportionate effect on higher harmonics.

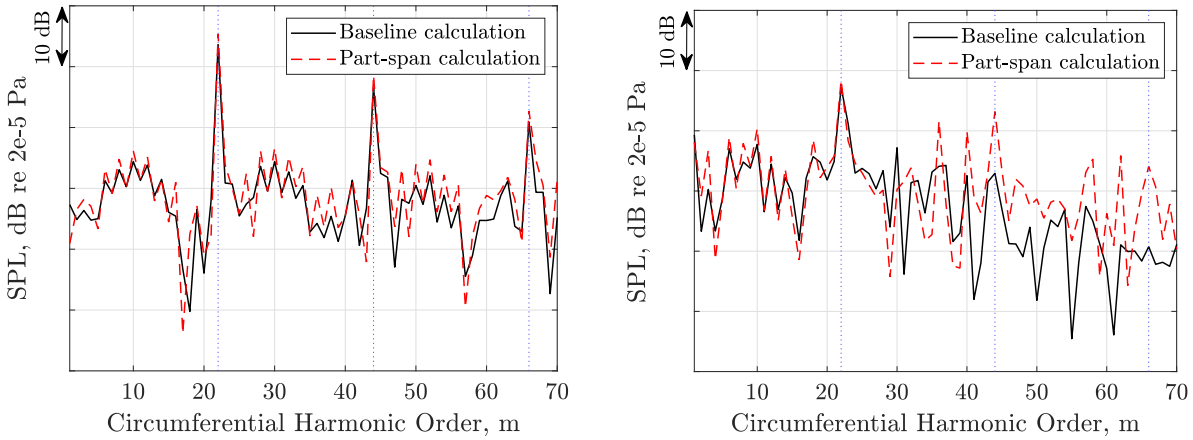

(a) Axial position upstream of the source plane by 5% of the duct outer wall radius.

(b) Axial position upstream of the source plane by 50% of the duct outer wall radius.

Fig. 13 The amplitude of different azimuthal harmonics following a spatial Fourier transform at 95% span and two axial positions for the baseline (–) and part-span (- -) calculations.

The previous comparison has been limited to data collected at snapshots during the calculation. A Fourier transform in time (over a full rotation of the fan/source) is now completed so that the amplitude between the cases can be more directly compared. In the present study, this is only presented at a limited number of enquiry points in the intake domain. There are two axially distributed arrays of points at 95% span. One is at the top of the nacelle ($\pi/2$) and one is at the bottom ($3\pi/2$). Furthermore, there are two rings of enquiry points azimuthally distributed at 95% span and two different axial locations. One is positioned slightly upstream of the source, but still close to it, and the other is at a point further upstream to understand the field after some propagation. The positions are the same as those used to present the data in Figure 13. As is discussed in Section V, the intention is to further this analysis for the entire in-duct computational domain which would allow for a deeper comparison and validation.

Figure 14 shows the amplitude of the pressure signal at blade passing frequency (EO= 22) along the axial array of points for both cases.

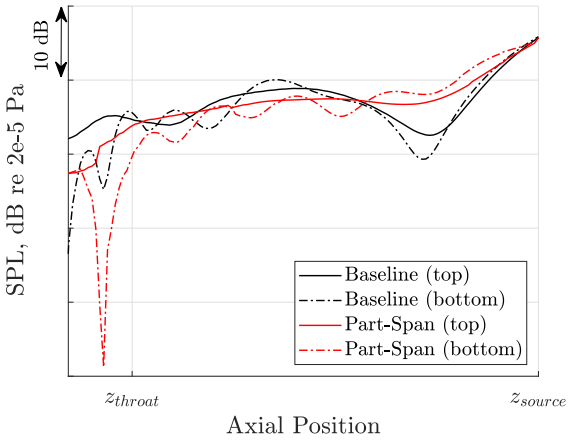

Fig. 14 SPL (dB) along an axial array of points at 95% span for blade passing frequency (EO= 22). Data is shown for two azimuthal positions referring to the top (solid line) and bottom (dot-dashed line) of the intake for the baseline (–) and part-span (–) calculations.

First observing the baseline calculation (black lines), there is a notable dip in amplitude upstream of the source. Wu and Wilson [31] complete a wavesplit of this data and highlight that this is due to interference of the first and second radial modes. The part-span calculation does not predict this dip in amplitude at either the top or bottom of the intake.

This could be due to the part-span approximation varying the axial wavenumbers of the radial modes meaning that they don't interfere in exactly the same manner.

Considering just the data at the top of the intake (solid lines), the general amplitude (other than at the previously mentioned dip) is predicted within 2 dB up to the intake throat. Also observed in both cases is the smooth variation in amplitude along the duct when compared to the data at the bottom of the intake.

At the bottom of the intake (dot-dashed lines), the amplitude varies more quickly along the duct. This is observed in both cases, though the variations are not in the same places axially along the duct. Once again, this could be due to wavenumber differences introduced by the part-span approximation meaning that the modes interfere constructively/destructively at different axial locations. If this variation is due to radial mode interference, the fact that the mean level and the peak-to-trough variation is similar in the two cases suggests that the amplitudes of each radial mode may be similar in the two cases but this needs to be confirmed using a wavesplit (Section V). Upstream of the throat, a significant dip in amplitude is observed for the part-span calculation. In the baseline calculation, a much smaller dip is observed. The reason for these dips is likely related to the higher flow velocity towards the bottom lip of the intake due to the inflow angle of attack. Further work is required to fully understand this.

Significant for a distorted acoustic field in the duct is the modal distribution at different frequencies. Considering a ring of equispaced enquiry points at 95% span, the mode distribution at any frequency can be determined by completing a Fourier transform in time (over a full cycle) followed by a Fourier transform in azimuthal space. This is completed at the first BPF and at two axial positions, considering the acoustic field close to the source, and following some upstream propagation in the duct.

Figure 15(a) shows this decomposition shortly upstream of the source plane (by 5% of the duct outer wall radius). Relative azimuthal mode order ($m - B$, where B is the number of blades) is centred on mode $m = 22$, which would be the only mode present at engine order 22 for a case with undistorted flow. Close to the source, this component has significantly higher (> 25 dB) amplitude than neighbouring modes. This is highlighted by both the part- and full-span calculations. The close agreement in this mode and the immediately neighbouring modes suggests that any additional effect of the fully coupled source in the baseline calculation is small. It also indicates that the impact of distortion for this case is not significant at the source, a conclusion also highlighted by Wu and Wilson [31]. At modes further from the $m - B = 0$ component, there are some differences in predicted amplitude. However, given these amplitudes are more than 35 dB lower than the peak, these variations are unlikely to have a major effect on the radiated sound field.

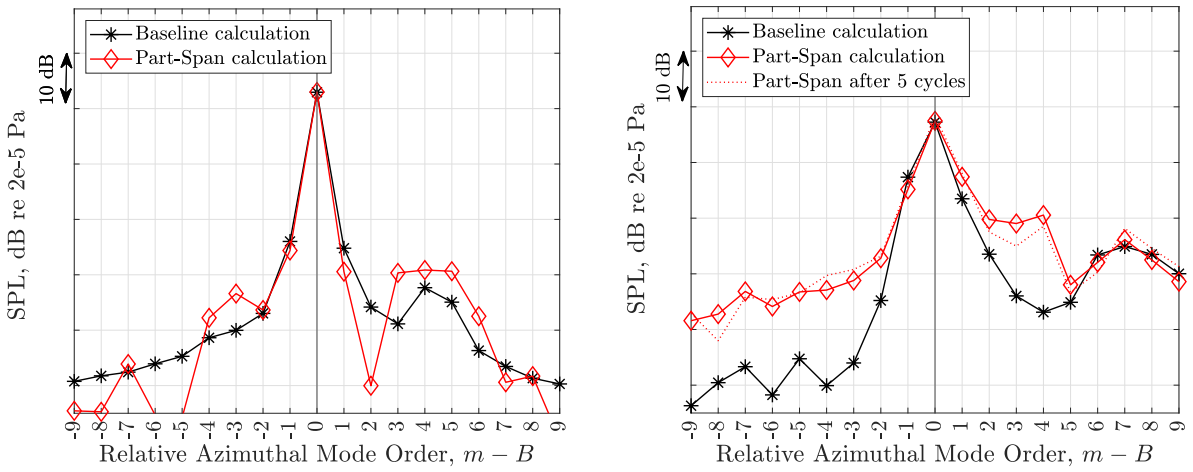

(a) Axial position upstream of the source plane by 5% of the duct outer wall radius.

(b) Axial position upstream of the source plane by 50% of the duct outer wall radius.

Fig. 15 Relative azimuthal mode ($m - B$) distribution at 95% span and the first BPF for the baseline (–) and part-span (–) calculations. In Figure 15(b), the red dotted line shows the result for the part-span calculation at a revolution prior to the 'final' result and is used to assess the level of convergence.

Figure 15(b) shows the azimuthal mode distribution at a position further upstream. Three data sets are shown. The black line is the mode distribution for the baseline calculation. Compared to Figure 15(a), the amplitude of the $m - B = 0$ component has decayed, while the amplitude of surrounding modes has increased. This highlights a mode

scattering effect due to the distortion, a phenomenon demonstrated in a number of previous studies, as described in Section I.A. A detailed discussion of the impact of distortion for this case is presented by Wu and Wilson [31].

Two results from the part-span calculation are presented on Figure 15(b). The solid red line shows the mode distribution computed after 6 full revolutions of the source, and the dotted line shows the mode distribution computed using data from one revolution earlier.

The later data (solid red line) predicts the same amplitude of the $m - B = 0$ mode when compared to the baseline calculation. The amplitudes of the immediately neighbouring modes ($m - B = \pm 1$) are predicted within 3 dB. For modes further from this point, there are some deviations which can be discussed in two parts considering positive, and negative components.

For the negative azimuthal components ($m - B < -1$), the part-span calculation over-predicts the amplitude of each mode. Given that these amplitudes are at least 20 dB lower than the amplitude of the dominant component, this may be insignificant in some cases. However, this result may indicate that the part-span calculation is not fully converged. To assess the convergence level, the dotted red line in Figure 15(b) highlights the same mode distribution data computed one cycle earlier. While small, there are some differences between the two cycles which suggests that the simulation may need to run for longer. It is expected that lower amplitude components will take longer to converge, and hence, this could explain observed differences at lower modes. Continuation of the calculation is suggested in the further work section (V).

At the positive azimuthal mode orders ($m - B > +1$), there are also some over-predictions of amplitude. This is particularly notable at $m - B = +4$, where an 18 dB difference is shown. To investigate this, approximate wavenumbers were calculated using a uniform axial mean flow approximation. These calculations demonstrated that the first radial mode passes through the cut-on/cut-off boundary at around this relative azimuthal mode ($m - B = +4$). Regarding the part-span approximation, the findings from Part I of this study [2] highlighted that, for modes close to the cut-on/cut-off boundary, greater error was introduced. Similarly, small differences between the two solvers can have a significant impact on the amplitude of modes close to the cut-on/cut-off boundary. Nevertheless, modes close to the cut-on/cut-off boundary typically have high amplitude but carry little acoustic power so this amplitude difference is expected to have relatively little effect on the radiated noise. At components higher than the estimated cut-on/cut-off boundary ($m - B > +4$), the part-span data matches the baseline calculation to within 2 dB.

III. Discussion

Based on the uniform duct CFD calculations, the approximation was shown to successfully predict the non-linear propagation of discrete tonal shock-associated noise for mid-to-high circumferential harmonics ($m = 11, 22$). This was particularly the case for the middle hub-to-tip ratio used ($\nu = 0.5$) which agreed with a negligible difference to the datum case. At the highest hub-to-tip ratio of 0.75, the approximation was still mostly sufficient at these circumferential harmonics, with only a small phase shift introduced. For the lowest circumferential harmonic tested ($m = 6$), the part-span approximation once again began to break down. There was a somewhat significant impact on both the amplitude and phase of the propagated shock wave. The impact was greatest for the high hub-to-tip ratio case and highlighted a potential limitation of the approximation. According to the findings of Part I of this study, it was anticipated that the error introduced would be greater on lower circumferential harmonics which was confirmed in this case. This is due to a more significant truncation of acoustic energy at the source plane as well as larger differences in the resultant axial wavenumbers.

The second test case presented a more realistic application of the part span approximation. The presence of a realistic, yet axisymmteric intake geometry, a small level of inflow distortion and a non-uniform source from a staggered fan highlighted how the approximation may be implemented in an applied setting. The part-span calculation was compared against a baseline calculation, completed by Wu and Wilson [31], which implemented a more conventional full-span methodology. A comparison between the two data sets highlighted that the part-span approximation could successfully propagate much of the acoustic data of interest, particularly surrounding the first BPF tone. At low circumferential harmonics of the buzz-saw spectrum, the part-span approximation compared well with the datum data. There were some notable deviations at very low circumferential harmonics which is consistent with the previous findings. While investigating the impact of distortion was not the main aim of the study, this test case demonstrated that the part-span approximation could capture some important distortion-interaction acoustic effects. For example, the modal distribution analysis in Figure 15 highlighted that the mode scattering effect due to distortion could be reasonably predicted by the part-span domain when compared to the baseline calculation. Key differences between the results were highlighted at the cut-on/cut-off boundary, which was anticipated according to the findings of Part I of the study. However, this may be

insignificant as modes close to this boundary typically carry little acoustic power.

At higher circumferential harmonics, there were some discrepancies which were mostly unexpected and require further investigation. It was also noticed that the initial propagation in the duct had some key differences. For example, as was shown in Figure 12, the initial decay in the baseline calculation of the shock field was not replicated by the part-span calculation where the amplitude remained more significant, and defined for a longer axial distance.

The part-span methodology is a possible reason for the discrepancies observed between the part-span and baseline calculations. However, there are other possible reasons which include:

- The calculations were performed using different CFD solvers. Although both are finite volume codes, the handling of shock waves will be different. Any difference in the shock-smoothing algorithm would be expected to have a disproportionate effect on higher harmonics.
- Figure 15(b) highlighted that some differences may be due to the part-span calculation not being sufficiently converged when compared to the baseline calculation.
- While evaluated to be small in the earlier discussion, there were small differences in the mean flow fields which may also be significant on acoustic propagation in the intake.

Addressing the high computational expense of high-fidelity tonal noise calculations is one of the aims of the study. In the intake domain, a computational mesh saving of 30% was achieved by applying the part-span approximation when compared with the full-span intake mesh of Wu and Wilson [31].

The methodology applied in test case B separated the propagation of acoustic content through the intake duct with the source calculation. Even for a full-span domain, it is expected that a two-part calculation method would achieve significant computational savings by splitting up an otherwise very large calculation into separate source and propagation calculations. The source calculation would encompass the whole computational domain but only resolve the acoustic field in the fan domain. The intake domain would have a mesh fine enough to capture the flow field and any potential flow distortion, but too coarse to propagate the acoustic content through the duct. For the propagation calculation, the intake would be considered separately using a high-resolution mesh sufficient to resolve the acoustic field. The steady and unsteady components of the pressure profile at the fan face would be extracted from the prior source calculation and used as an input for the propagation calculation applying the methodology validated in test case B.

This two-part method offers significant savings as the domain becomes effectively shorter and the mesh count is smaller in both calculations. In the source calculation, the time to convergence is reduced because acoustic content no longer has to propagate upstream through the intake duct. In the propagation calculation, the fan is not considered, significantly reducing the mesh count. A part-span version of the propagation calculation is applied in test case B of this paper. This two-part method on its own is expected to achieve a computational saving of 45%, and combined with the part-span approximation with a hub-to-tip ratio of 0.5 would achieve a 60% saving when compared with the equivalent calculation of Wu and Wilson [31].

IV. Conclusions

The part-span approximation was applied to an axisymmetric, but otherwise realistic, intake geometry with non-uniform inflow and was shown to accurately capture the most significant effects of inflow distortion. The highest amplitude scattered modes are predicted to within around 4 dB of the baseline solution but the detailed behaviour, partly due to the radial phasing of the modes, was less accurate in some parts of the duct.

Further work is required to determine the accuracy of the part-span approximation for far-field noise predictions.

A two-part calculation method has been proposed which potentially offers a 45% computational saving. In addition, the part-span approximation reduces the mesh count in the intake domain by around 30%. Applied in conjunction with each other, the total saving is predicted to be 60%.

The part-span approximation was applied to a number of academic test cases with high amplitudes leading to non-linear propagation. In most cases, the part-span results matched the datum results well. The part-span approximation was demonstrated to break down for high-amplitude non-linear propagation of low circumferential harmonics ($m = 6$) where a significant proportion of the acoustic energy is neglected. It is noted that in the more realistic case, test case B, the amplitude of these low circumferential harmonics was lower and could be more accurately resolved by the part-span approximation, although significant errors were still observed for circumferential harmonics lower than $m = 5$.

As was established in Part I of the study, for acoustic modes that are cut-off, or close to the cut-on/cut-off boundary, further care is required and significant error can be introduced. This is expected to have a limited effect on radiated sound, as acoustic modes close to the cut-on/cut-off boundary typically carry little acoustic power.

The results presented demonstrate behaviour consistent with the types of error established in Part I of this study.

Further work is required to confirm that this behaviour holds across all intake geometries and operating conditions.

V. Future work

Many areas of future work were highlighted in this study and include:

- Generate a new baseline calculation for test case B using exactly the same CFD solver and methodology as for the part-span calculation.
- Extend the calculation time for the part-span calculation in test case B. A potential advantage of a part-span methodology for realistic cases is the requirement for simulations to run for fewer cycles of rotation to sufficiently propagate the acoustic source in the intake. However, in test case B, it was highlighted that some differences between the part-span and datum results could be the result of a simulation that was not fully converged.
- The comparison of the part-span approximation with the full-span calculation in test case B was limited to unsteady pressure data at a discrete, and limited, number of enquiry points in the domain. It would be beneficial to generate a frequency-based description of the acoustic field in the intake, as completed by Wu and Wilson [31]. This would permit a frequency-based Fourier-Bessel wavesplit, as performed for test case A.
- Test case B considered a shallow angle of attack, such that the effect of distortion was relatively low. Hence, there is interest in applying this methodology to non-axisymmetric intake geometries and steeper inflow angles to further explore the impact of distortion. Assessing the impact of a part-span approximation on intakes with acoustically lined duct walls is also of interest.

Acknowledgments

The work presented in this paper is funded through the PhD work of the first author which is financially supported by the University of Southampton and Rolls-Royce plc. The authors wish to acknowledge Howoong Namgoong, the wider noise team and the CFD team at Rolls-Royce for their continued support and technical discussion. Rolls-Royce are also acknowledged for data provided throughout this project. The authors acknowledge the use of the IRIDIS High Performance Computing Facility, and associated support services at the University of Southampton.

References

[1] Moreau, S., "Turbomachinery Noise Predictions: Present and Future," *Acoustics*, Vol. 1, No. 1, 2019, pp. 92–116. https://doi.org/10.3390/acoustics1010008.

[2] Binns, J. S. P., Wu, L., and Wilson, A. G., "Part-Span Approximation of Tone Noise Propagation in an Aeroengine Intake. Part I: Linear Propagation," *30th AIAA/CEAS Aeroacoustics Conference, 2024*, 2024.

[3] Morfey, C.L., and Fisher, M.J., "Shock-Wave Radiation From Supersonic Ducted Rotor," *Aeronautical Journal*, Vol. 74, No. 715, 1970, pp. 579–585. https://doi.org/10.1017/s0001924000049095.

[4] McAlpine, A., and Fisher, M. J., "On the prediction of "Buzz-saw" noise in aero-engine inlet ducts," *Journal of Sound and Vibration*, Vol. 248, No. 1, 2001, pp. 123–149. https://doi.org/10.1006/jsvi.2001.3770.

[5] Stratford, B., and Newby, D., "A New Look at the Generation of Buzz-saw Noise," *44th AIAA Aeroacoustics Conference*, 1977, pp. 1–23. https://doi.org/https://doi.org/10.2514/6.1977-1343.

[6] McAlpine, A., Fisher, M. J., and Tester, B. J., ""buzz-saw" noise: A comparison of measurement with prediction," *Journal of Sound and Vibration*, Vol. 290, No. 3-5, 2006, pp. 1202–1233. https://doi.org/10.1016/j.jsv.2005.05.028.

[7] Hawkings, D., "Multiple tone generation by transonic compressors," *Journal of Sound and Vibration*, Vol. 17, No. 2, 1971, pp. 241–250. https://doi.org/10.1016/0022-460X(71)90458-5.

[8] Aerospace Technology Institute, "UHBR Engine Roadmap," Tech. rep., Aerospace Technology Institute, 2021.

[9] McAlpine, A., and Fisher, M. J., "On the prediction of "buzz-saw" noise in acoustically lined aero-engine inlet ducts," *Journal of Sound and Vibration*, Vol. 265, No. 1, 2003, pp. 175–200. https://doi.org/10.1016/S0022-460X(02)01446-3.

[10] McAlpine, A., Fisher, M. J., and Tester, B. J., ""Buzz-saw" noise: A comparison of modal measurements with an improved prediction method," *Journal of Sound and Vibration*, Vol. 306, No. 3-5, 2007, pp. 419–443. https://doi.org/10.1016/j.jsv.2007.04.053.

[11] McAlpine, A., Schwaller, P. J., Fisher, M. J., and Tester, B. J., "Buzz-saw noise: Prediction of the rotor-alone pressure field," *Journal of Sound and Vibration*, Vol. 331, No. 22, 2012, pp. 4901–4918. https://doi.org/10.1016/j.jsv.2012.06.009, URL http://dx.doi.org/10.1016/j.jsv.2012.06.009.

[12] Pickett, G. F., and Sofrin, T. G., "Multiple pure tone noise generated by fans at supersonic tip speeds," *Pratt & Whitney Aircraft*, 1970.

[13] Achunche, I., Astley, R. J., Sugimoto, R., and Kempton, A., "Prediction of Forward Fan Noise Propagation and Radiation from Intakes," *15th AIAA/CEAS Aeroacoustics Conference (30th AIAA Aeroacoustics Conference)*, AIAA, 2009.

[14] Astley, R. J., Sugimoto, R., and Mustafi, P., "Computational aero-acoustics for fan duct propagation and radiation. Current status and application to turbofan liner optimisation," *Journal of Sound and Vibration*, Vol. 330, No. 16, 2011, pp. 3832–3845. https://doi.org/10.1016/j.jsv.2011.03.022, URL http://dx.doi.org/10.1016/j.jsv.2011.03.022.

[15] Schwaller, P. J., Tester, B. J., and Henshaw, D. G., "The effects on fan noise of inlet steady flow distortion," *3rd AIAA/CEAS Aeroacoustics Conference*, 1997, pp. 40–46. https://doi.org/10.2514/6.1997-1590.

[16] Schwaller, P. G., Baker, N. J., Tomlinson, J. D., Sijtsma, P., and Hemmings, R., "Noise validation of model fan rig with engine," *Collection of Technical Papers - 12th AIAA/CEAS Aeroacoustics Conference*, Vol. 2, No. May, 2006, pp. 1014–1025. https://doi.org/10.2514/6.2006-2479.

[17] Winkler, J., Reimann, C. A., Gumke, C. D., Ali, A. A., and Reba, R. A., "Inlet and aft tonal noise predictions of a full-scale turbofan engine with bifurcation and inlet distortion," *23rd AIAA/CEAS Aeroacoustics Conference, 2017*, , No. June, 2017, pp. 1–14. https://doi.org/10.2514/6.2017-3034.

[18] Sanjosé, M., Moreau, S., Pestana, M., and Roger, M., "Effect of weak outlet-guide-vane heterogeneity on rotor-stator tonal noise," *AIAA Journal*, Vol. 55, No. 10, 2017, pp. 3440–3457. https://doi.org/10.2514/1.J055525.

[19] Peake, N., and Parry, A. B., "Modern challenges facing turbomachinery aeroacoustics," *Annual Review of Fluid Mechanics*, Vol. 44, 2011, pp. 227–248. https://doi.org/10.1146/annurev-fluid-120710-101231.

[20] Doherty, M., and Namgoong, H., "Impact of turbofan intake distortion on fan noise propagation and generation," *22nd AIAA/CEAS Aeroacoustics Conference, 2016*, 2016, pp. 1–18. https://doi.org/10.2514/6.2016-2841, URL http://dx.doi.org/10.2514/6.2016-2841.

[21] Daroukh, M., "Effect of distortion on modern turbofan tonal noise," 2017, pp. 1–204.

[22] Daroukh, M., Moreau, S., Gourdain, N., Boussuge, J. F., and Sensiau, C., "Tonal noise prediction of a modern turbofan engine with large upstream and downstream distortion," *Journal of Turbomachinery*, Vol. 141, No. 2, 2019. https://doi.org/10.1115/1.4042163.

[23] Prinn, A. G., Sugimoto, R., and Jeremy Astley, R. J., "The effect of steady flow distortion on noise propagation in turbofan intakes," *22nd AIAA/CEAS Aeroacoustics Conference, 2016*, 2016, pp. 1–14. https://doi.org/10.2514/6.2016-3028.

[24] James, A. O., "Buzz-Saw Noise Prediction for Axisymmetric and Drooped Turbofan Intakes by," , No. December, 2020.

[25] Sugimoto, R., James, A. O., McAlpine, A., and Astley, R. J., "CFD/CAA coupling for the prediction of fan tone noise propagation and radiation through a drooped intake," *28th AIAA/CEAS Aeroacoustics Conference, 2022*, 2022, pp. 1–15. https://doi.org/10.2514/6.2022-3100.

[26] Winkler, J., Aaron Reimann, C., Reba, R., and Gilson, J., "Turbofan inlet distortion noise prediction with a hybrid CFD-CAA approach," *20th AIAA/CEAS Aeroacoustics Conference*, Vol. 3, No. June, 2014. https://doi.org/10.2514/6.2014-3102.

[27] Daroukh, M., Polacsek, C., and Chelius, A., "Shock wave generation and radiation from a turbofan engine under flow distortion," *AIAA Journal*, Vol. 58, No. 2, 2020, pp. 787–801. https://doi.org/10.2514/1.J058799, URL https://doi.org/10.2514/1.J058799.

[28] Daroukh, M., Moreau, S., Gourdain, N., Boussuge, J. F., and Sensiau, C., "Influence of distortion on fan tonal noise," *22nd AIAA/CEAS Aeroacoustics Conference, 2016*, 2016.

[29] Tyler, J. M., and Sofrin, T. G., "Axial flow compressor noise studies," SAE Technical Paper 620532, 1962. https://doi.org/10.4271/620532.

[30] Astley, R. J., Sugimoto, R., Gabard, G., Norde, E., Grift, E. J., and Bocquier, M., "The effect of steady flow distortion on mode propagation in a turbofan intake," *20th AIAA/CEAS Aeroacoustics Conference*, , No. June, 2014, pp. 1–22. https://doi.org/10.2514/6.2014-3113.

[31] Wu, L., and Wilson, A. G., "Fan Buzz-Saw Noise under Intake Flow Distortion: a Computational Study," *30th AIAA/CEAS Aeroacoustics Conference, 2024*, 2024.

[32] Wilson, A. G., and Coupland, J., "Numerical prediction of aeroengine fan stage tone noise sources using CFD," *ECCOMAS 2004 - European Congress on Computational Methods in Applied Sciences and Engineering*, , No. July, 2004.

[33] Coupland, J., Wilson, A. G., Pollard, N., Uellenberg, S., Breard, C., and Diamond, J., "Demonstration of a CFD-CAA methodology to predict buzz-saw noise propagation to the aircraft," *13th AIAA/CEAS Aeroacoustics Conference (28th AIAA Aeroacoustics Conference)*, 2007, pp. 1–15. https://doi.org/10.2514/6.2007-3517.

[34] Wu, L., Kim, J.-W., Wilson, A. G., and Shahpar, S., "Automatic Design Optimization of a Transonic Compressor Rotor for Improving Aeroacoustic and Aerodynamic Performance," *Journal of Turbomachinery*, Vol. 144, No. 8, 2022. https://doi.org/10.1115/1.4053916.

[35] Wilson, A. G., "A Method for Deriving Tone Noise Information from CFD Calculations on the Aeroengine Fan Stage," *RTO AVT Symposium on "Ageing Mechanism and Control: Part A - Developments in Compurational Aero- and Hydro-Acoustics"*, 2001.